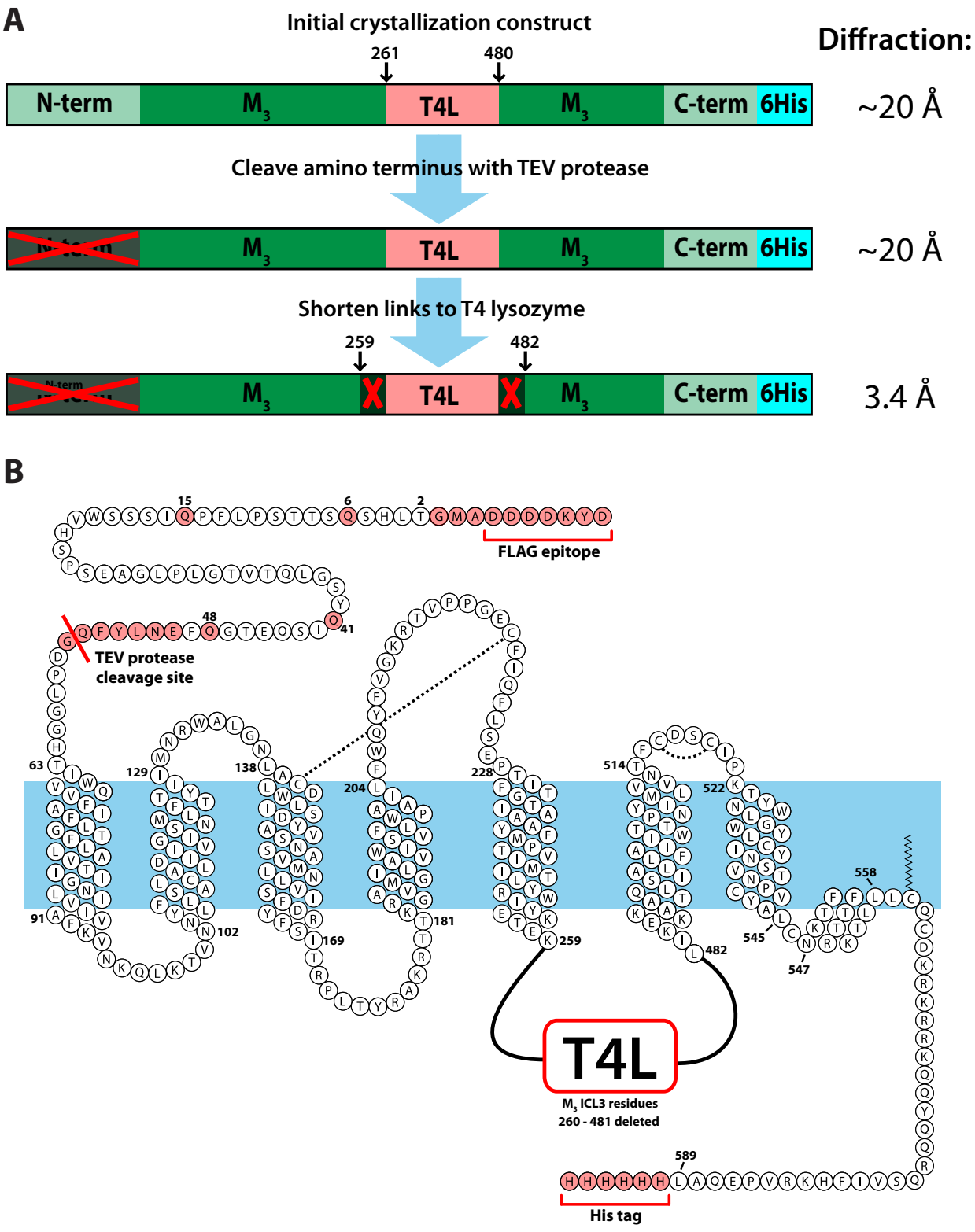

Figure S1. Crystallography construct design. A variety of crystallization constructs were tested (**a**), with best results obtained using a shortened link to T4 lysozyme relative to that tested initially. The final crystallization construct is shown in (**b**)

with all modifications to the wild-type protein indicated in red. In the amino terminal domain four potential N-glycosylation sites (N6, N15, N41, N48) were replaced with glutamine, and M_3 residues 50-56 were replaced with a TEV protease site. K259 and L482 correspond to Ballesteros-Weinstein numbers 5.67 and 6.27, respectively. Amino acid numbers refer to the wild-type rat M_3 receptor sequence. We used the rat rather than the human M_3 receptor because the rat version of this receptor subtype has been the subject of very extensive biochemical, mutagenic, and pharmacological studies. Differences between rat and human M_3 receptor amino acid sequences are minimal, and almost exclusively confined to unresolved parts of the structure such as the third intracellular loop and the extended N-terminus.

Key residues including N1.50, D2.50, D3.49, E6.30, N7.49, and Y7.53 were included in the crystallization construct, and with the exception of E6.30 each of these was clearly resolved in the electron density. These residues adopt very similar conformations in both the M_2 and M_3 receptors. In the M_3 receptor, like the M_2 receptor, D3.49 is H-bonded to Y3.60.

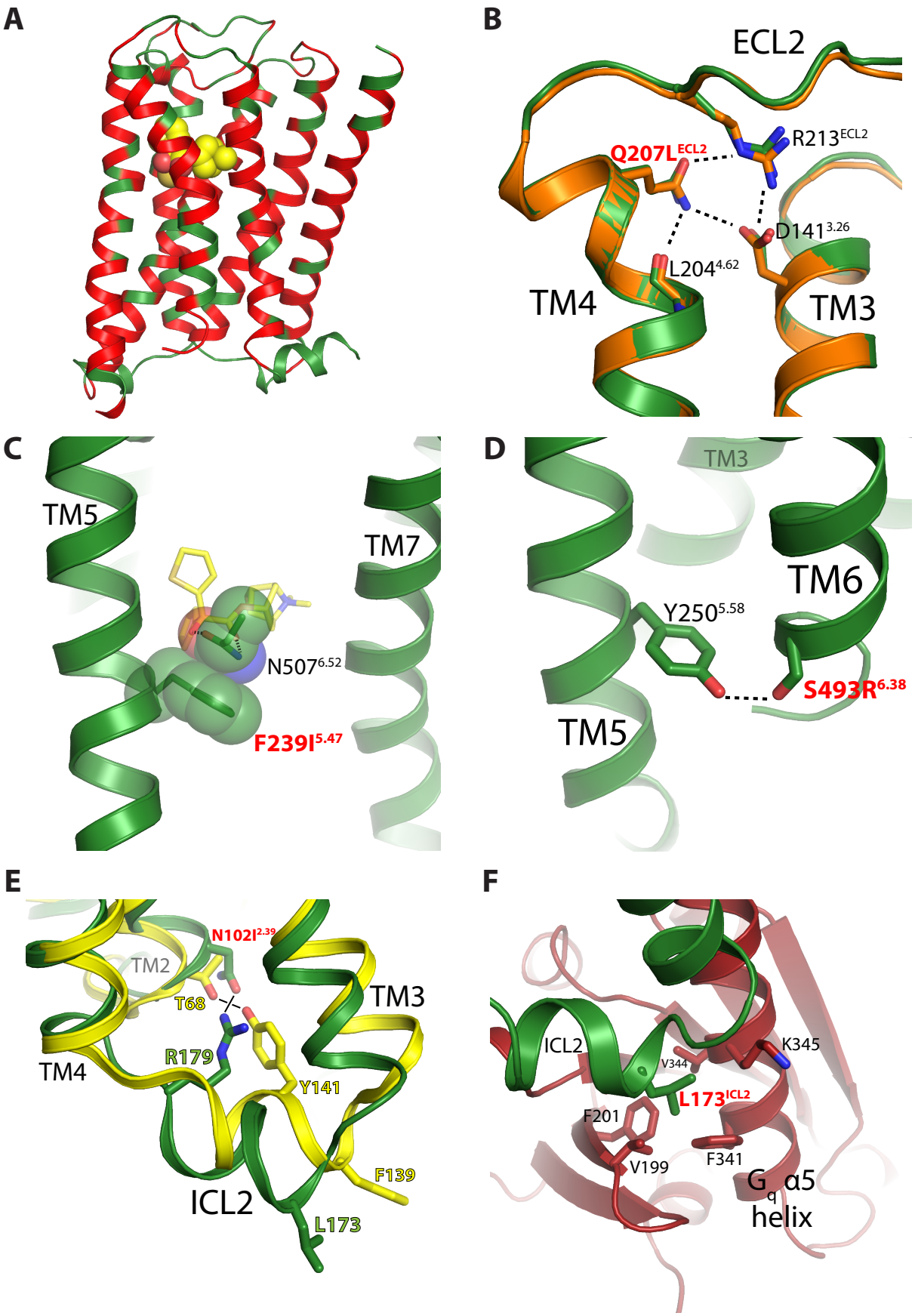
A
B
ECL2
R213ECL2
Q207LECL2
D1413.26
L2044.62
TM4
TM3
C
TM5
TM7
N5076.52
F239I5.47
D
TM3
TM6
Y2505.58
S493R6.38
TM5
E
N102I2.39
TM2
T68
TM3
R179
TM4
Y141
F139
ICL2
L173
F
ICL2
K345
V344
L173ICL2
F201
V199
F341
Gq α5
helix

Figure S2. Structural insights into mutagenesis data. Members of the mAChR family, particularly the M_3 receptor, have been subjected to some of the most extensive mutagenesis studies in the GPCR field. We present here several examples of how the new M_3 receptor structure facilitates the interpretation of the effects of specific M_3 receptor point mutations.

(**a**) Structure of the M_3 receptor with sites of previously characterized single-site point mutations highlighted in red. The orthosteric site is indicated by the ligand tiotropium (yellow spheres for carbons, red for oxygens).

(**b**) The M_3 Q207L mutation led to significant impairments of both ligand binding and receptor activation[1]. Q207 is located on the extracellular end of TM4, which exhibits a pronounced bend in both the M_2 (orange) and M_3 (green) mAChRs. This bend is stabilized by a hydrogen bond from the Q207 (Q163 in M_2) side chain to the L204 backbone peptide carbonyl. This bond is part of a polar interaction network involving four residues absolutely conserved within the mAChR family. The detrimental effects of the Q207L mutation suggest that this interaction network is important for normal function of the receptor. The TM4 bend may be important for maintaining the proper structure of extracellular loop 2, to which it is connected. Consistent with the importance of this polar interaction network, mutation of M_3 R213 to a variety of residues also resulted in impaired receptor function[1], and mutation of D99$^{3.26}$ to alanine in the M_1 mAChR led to impairment of binding to ^{3}H NMS and acetylcholine[2]. Studies with mutant human M_1 receptors also showed that the residue corresponding to M_3 R213 (M_1 R171) plays a role in stabilizing a receptor conformation that slows down ligand (QNB) dissociation[2]. Somewhat surprisingly, however, mutation of M_1 Q165 (equivalent to M_3 Q207) to alanine caused only slight impairments in receptor activation[2] and ligand binding[3].

(**c**) The M_3 F239I$^{5.47}$ mutation was shown to cause a significant decrease in receptor expression and to completely abolish both ligand binding and receptor activation[4]. In the structure of the M_3 receptor (and also of the M_2 receptor) this residue engages in few direct contacts with the ligand, but provides a flat surface for stacking of N507$^{6.52}$, a residue conserved among all five mAChRs, that directly hydrogen bonds to tiotropium. The F239I mutation likely results in repositioning of N507, so that the receptor-ligand hydrogen bond pair cannot form. Studies with mutant human M_1 receptors indicated that the M_1 F197A$^{5.47}$ point mutation also led to significant reductions in NMS binding affinity and receptor expression levels (note, however that the affinity for QNB was not affected by this point mutation)[2]. In this figure van der Waals spheres are shown to illustrate the tight packing of N507 against F239.

(**d**) Replacement of M_3 S493$^{6.38}$ with either arginine[4] or glycine[5] had little effect on agonist and antagonist binding affinities, but severely interfered with productive G protein signaling[4,5], suggesting this residue plays an important role in receptor-G protein interactions. S493 is conserved in the M1, M_3, and M5 receptors, but not among the M_2 or M_4 subtypes. The structure of the M_3 receptor shows that this residue engages in a

hydrogen bond with a highly conserved TM5 tyrosine residue, Y250$^{5.58}$. This bond would likely be disrupted by the mutation.

(**e**) M_3 N102$^{2.39}$ is located at the cytoplasmic end of TM2, and may hydrogen bond to R179 in the second intracellular loop. The N102I point mutation caused essentially no change in ligand binding affinities, but inhibited agonist-induced receptor signaling[4], suggesting that N102, like S493 discussed above, may play a role in G protein coupling. By interacting with R179, N102 may help control the placement of intracellular loop 2, an important receptor/G protein contact surface. Interestingly, the residue analogous to N102 in the β_2 adrenergic receptor (T68) does not directly interact with the G protein G_s in the recently solved complex[6], but hydrogen bonds to Y141 in ICL2. This interaction appears to stabilize the position of F139, which binds a hydrophobic pocket on the G protein. In M3, N102 appears to play an analogous role, stabilizing the position of L173, the residue equivalent to F139 in the β_2AR. In this figure the M_3 receptor is in green, superimposed on the β_2AR in yellow.

(**f**) M_3 L173 was recently identified as an important M_3/G_q contact site in a cross-linking study[7], and previous mutagenesis experiments also noted the importance of this residue in muscarinic and adrenergic receptor signaling[8]. The recent structure of the β_2 adrenergic receptor-G_s complex showed that the analogous residue in the β_2 receptor (F139) is buried into a hydrophobic pocket of the G_s α-subunit[6]. Prompted by this observation, we used the program Modeller[9] to build a composite homology model of an M_3-G_q complex using the inactive M_3 receptor structure and the β_2 receptor signaling complex as templates. The resulting model suggests that M_3 receptor activation may enable L173 to bind the α-subunit of G_q in a manner similar to that observed for the β_2 F139-Gα_s interaction, consistent with the results of M_3-G_q cross-linking[7] and site-directed mutagenesis studies[8]. Green, M_3 receptor; red, Gα_q.

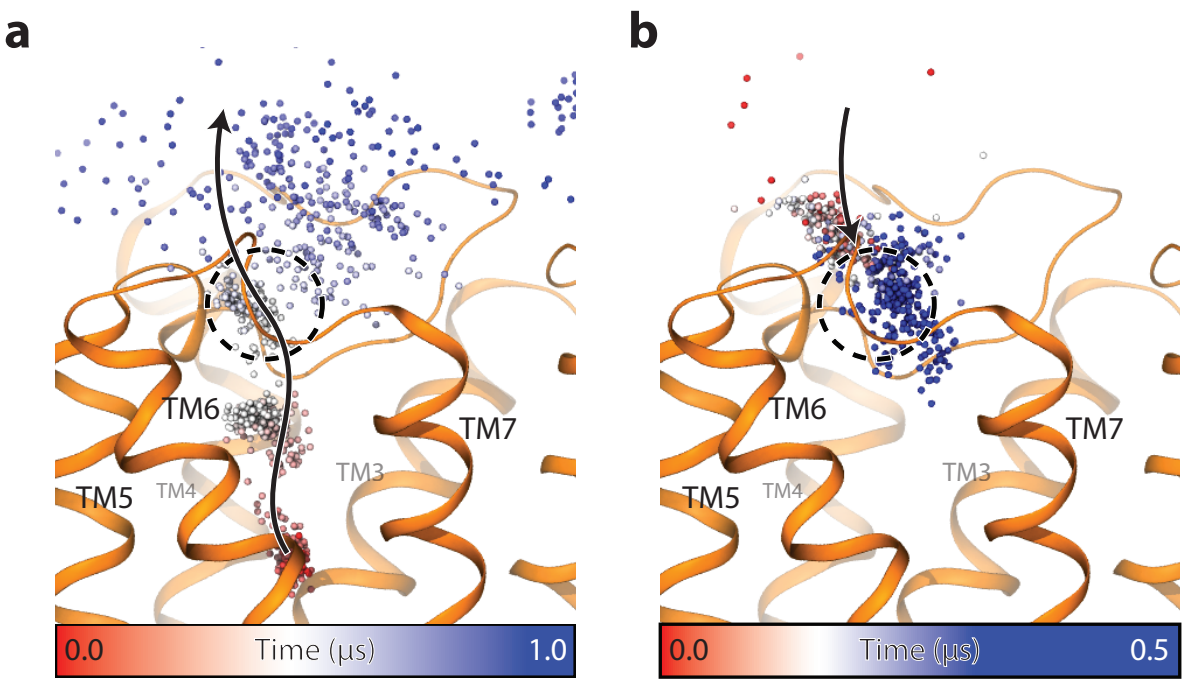

Figure S3. Binding/dissociation of tiotropium to the M_2 receptor.
Binding pathway for the M_2 receptor, as inferred from MD simulations (*cf.* Fig 3a and 3b, which show similar data for the M_3 receptor). (**a**) When the ligand is pushed out of the binding pocket (with no favored direction), it pauses in the extracellular vestibule. Colored spheres represent positions of the ligand's tropane C3 atom at successive points in time. (**b**) When the ligand is placed in bulk solvent and allowed to diffuse freely about the receptor, it eventually binds to the same site in the extracellular vestibule; our simulations are not sufficiently long for it to proceed into the binding pocket.

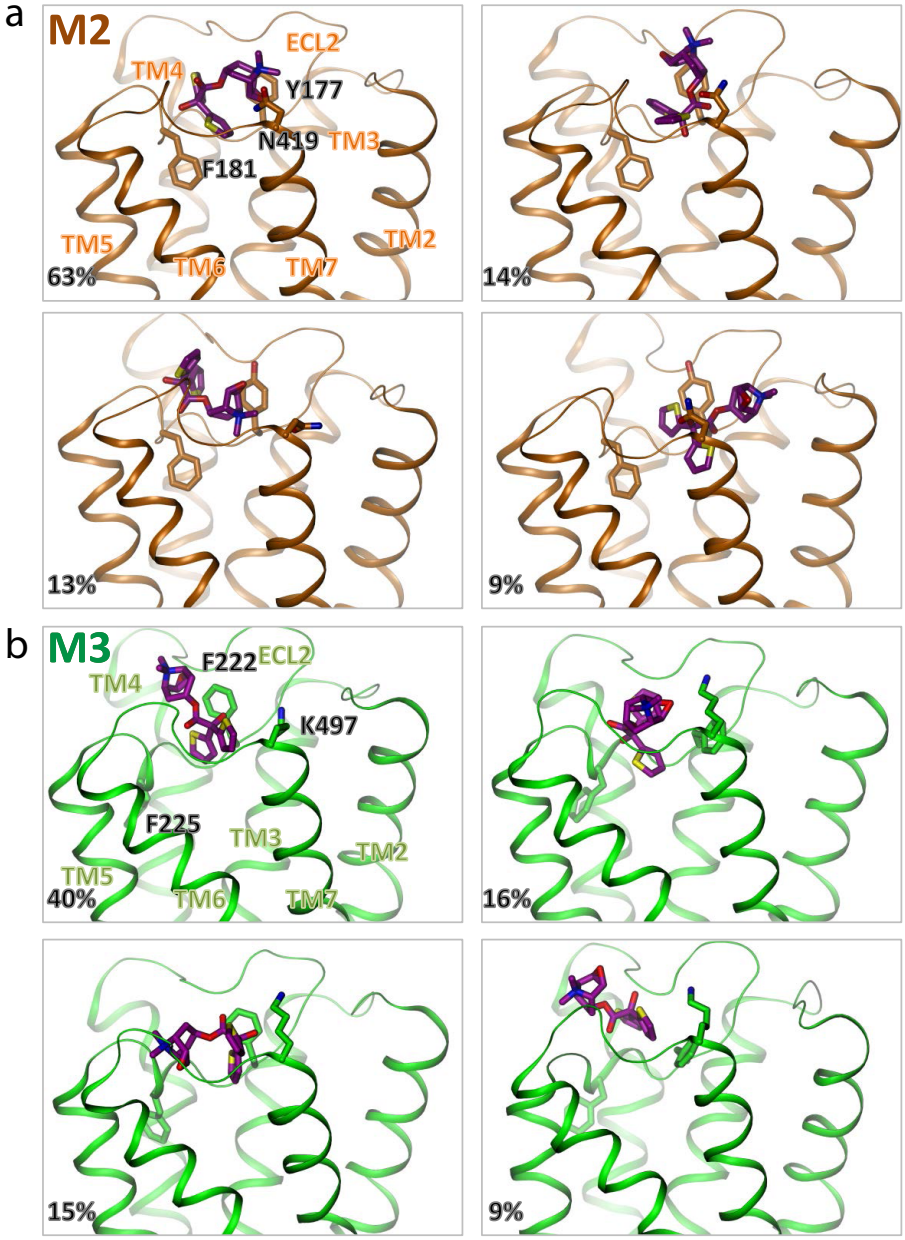
a
M2
ECL2
TM4
Y177
N419
TM3
F181
TM5
TM2
TM6
TM7
63%
14%
13%
9%
b
M3
F222
ECL2
TM4
K497
F225
TM3
TM2
TM5
TM6
TM7
40%
16%
15%
9%
c
O
OH
S
O
N
+
O
S

Figure S4. Tiotropium assumes a variety of poses in the extracellular vestibules of the M_2 and M_3 receptors. (**a**), M_2 (orange) with the four most common vestibule-bound poses of tiotropium (purple) during the 14.2-μs spontaneous binding simulation (Supplementary table 4, condition D). (**b**), M_3 (green) with the four most common vestibule-bound poses of tiotropium (purple) during the 16.0-μs spontaneous binding simulation (Supplementary table 4, condition E). The percentage in the bottom left corner of each image represents the percentage of vestibule-bound time spent in that particular pose. (**c**), The black arrows indicate the atoms used for clustering the ligand positions into poses. Low confidence should be assigned to relative frequencies of the various poses, given the amount of simulation performed and potential sensitivities to force field parameters. See Supplementary Methods for details.

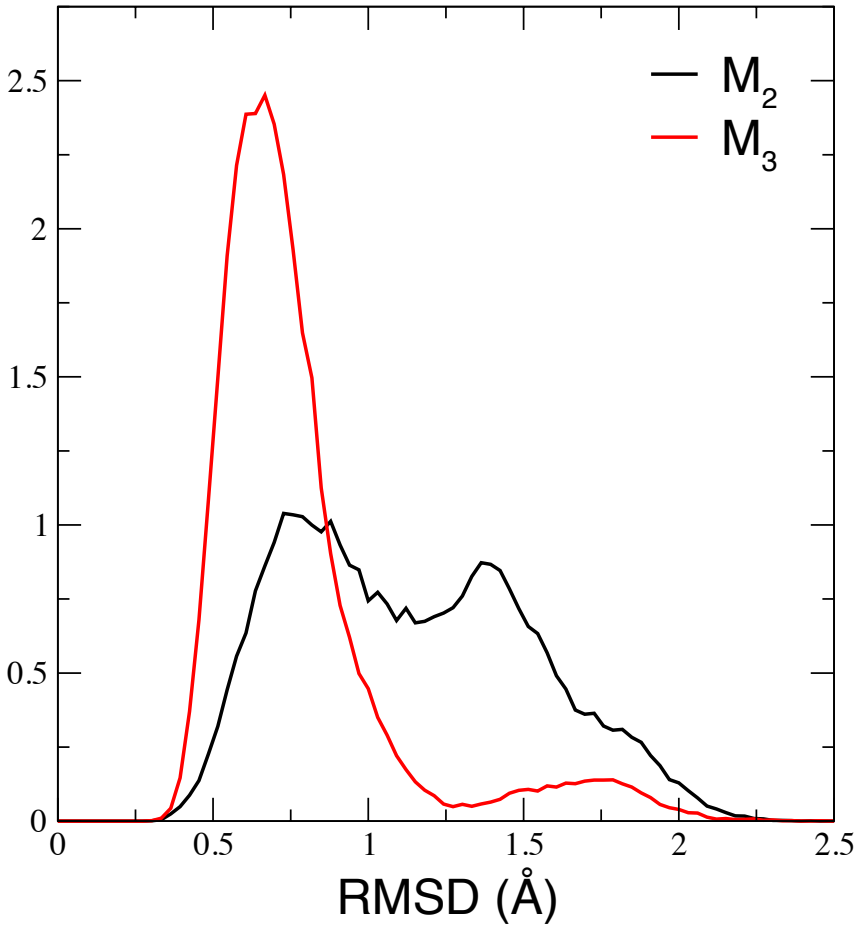

Figure S5. Extracellular loop 2 (ECL2) is more mobile in the M_2 receptor than in the M_3 receptor. The curves represent distributions (i.e., normalized histograms) of the root mean square deviation (RMSD) from the crystal structures of ECL2 in simulations of the M_2 (black) and M_3 (red) receptors. RMSDs were computed for backbone atoms of the portions of ECL2 near the binding pocket (residues 177 to 188 in M_2 and 221 to 232 in M_3), after best fit alignment, for the first 10 μs of simulations of tiotropium-bound M_2 and M_3 receptors (Supplementary table 4, conditions B and C). The RMSD distribution of ECL2 in M_2 is substantially broader than that of M_3, indicating more dynamical fluctuation in this region for the M_2 receptor. This difference may contribute to tiotropium's slower off-rate from the M_3 receptor. The behavior of ECL2 in a simulation of M_2 bound to its cocrystallized ligand, QNB (Supplementary Table 4, condition A), was similar to that in the tiotropium-bound M_2 simulation shown here.

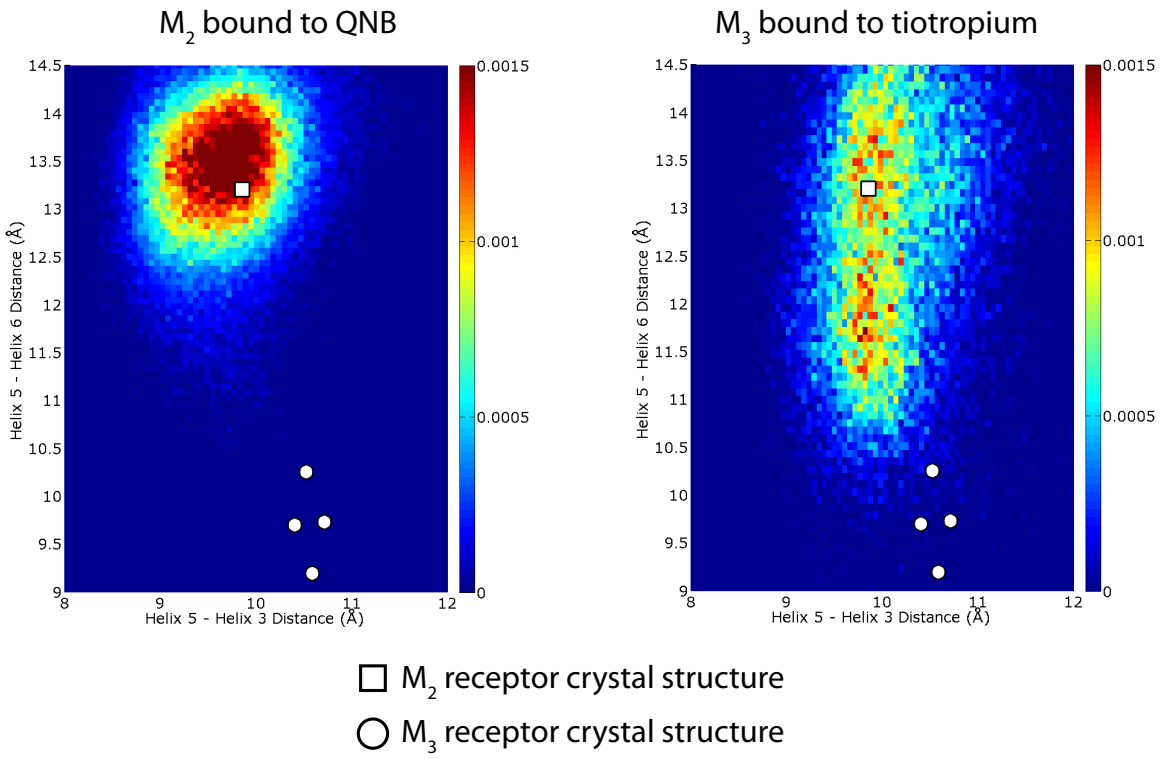

Figure S6. TM5 motion viewed by molecular dynamics. Observed conformations of TM5 in simulations of the M_2 and M_3 receptors with the T4 lysozyme removed. Two-dimensional histograms of an M_2 simulation and an M_3 simulation, with each receptor bound to its co-crystallized ligand. The axes are the same as in Fig. 3c: the vertical axis indicates the distance between the α carbons of residues 5.62 and 6.37, and the horizontal axis the distance between the α carbons of residues 5.62 and residue 3.54. The color of each pixel represents the fraction of all simulation frames (snapshots) that fall into the corresponding bin. In the M_2 simulation, TM5 is mostly in a conformation similar to that seen in the M_2 crystal structure. In the M_3 simulation, TM5 is more mobile; it fluctuates between conformations similar to those seen in the M_3 crystal structure and conformations more similar to those seen in the M_2 crystal structure.

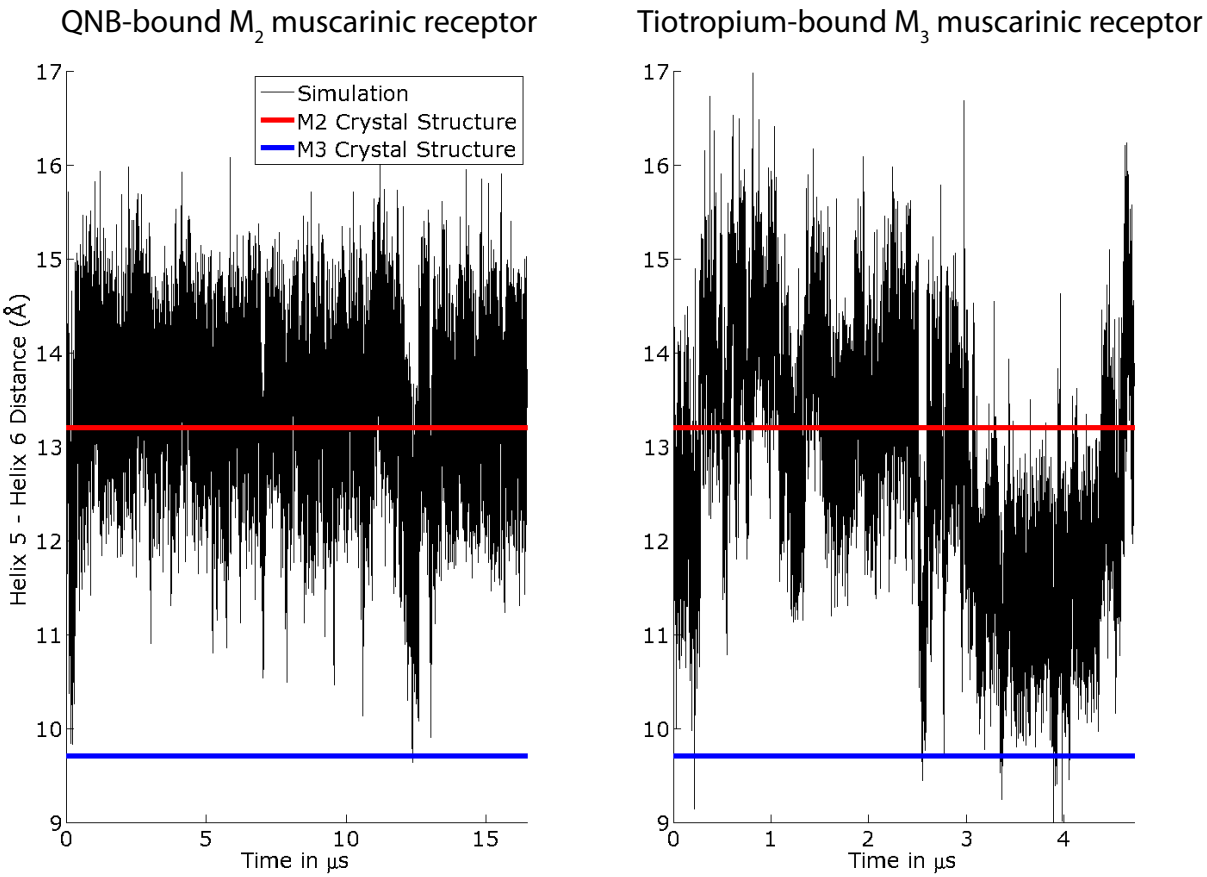

Figure S7. Time trace of TM5 motion. Distance between residues 5.62 and 6.37 (corresponding to the vertical axis in Fig. S6 and Fig. 4c) as a function of time for the M_2 and M_3 simulations illustrated in Fig. S6. The blue line corresponds to the average distance for the four M_3 molecules in the crystal structure.

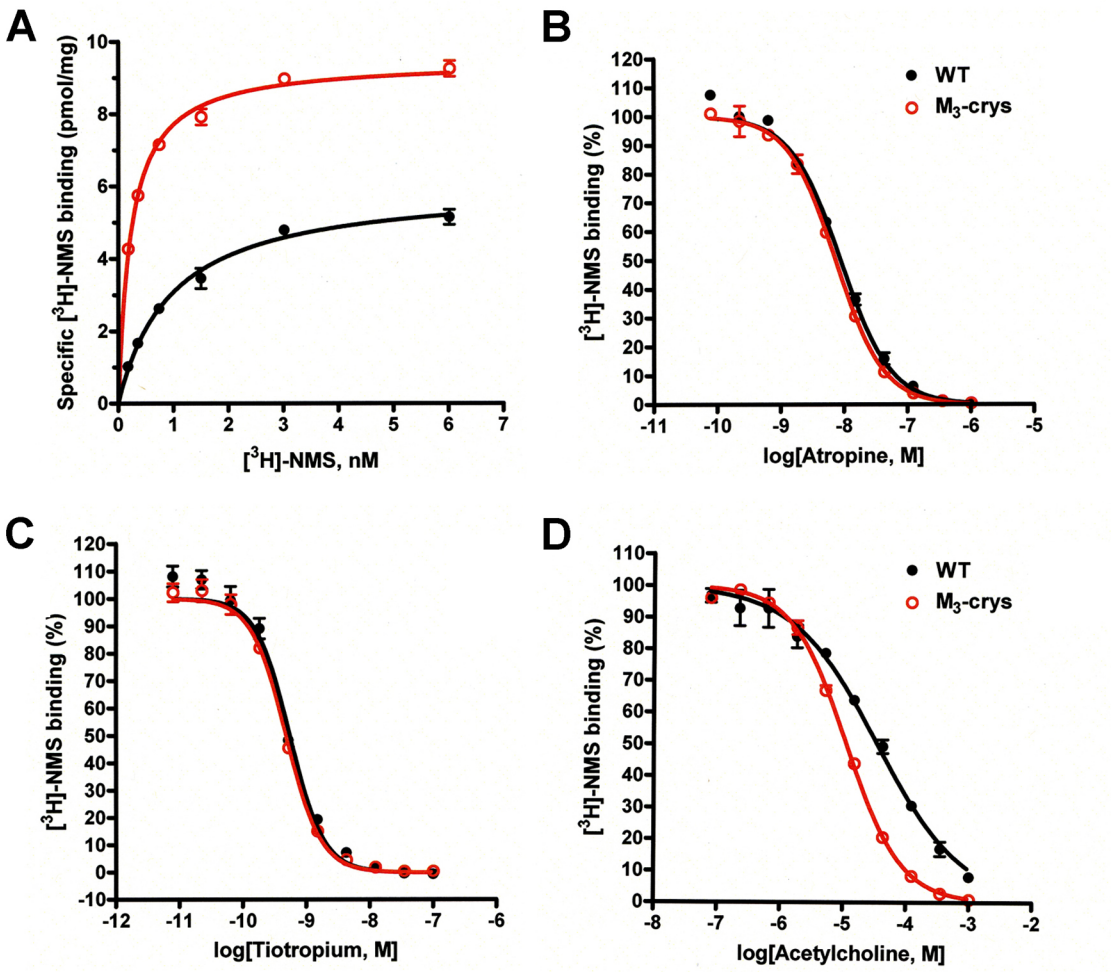

Figure S8. Radioligand binding studies. **(a)** Saturation binding curves of specific [^{3}H]NMS binding to the wild type M_3 receptor (rat) and the modified M_3 receptor construct used for crystallization studies (M_3-crys). **(b-d)** Displacement of [^{3}H]NMS binding by atropine **(b)**, tiotropium **(c)**, and acetylcholine **(d)**. Binding assays were carried out using membranes prepared from transfected COS-7 cells. The [^{3}H]NMS concentration used in the competition binding assays was 0.5 nM. Curves are representative of 2-4 experiments carried out in duplicate (for experimental details, see Supplementary Methods). [^{3}H]NMS K_D and B_{max} values and K_i/IC_{50} values for the three cold ligands used are given in supplementary table 1.

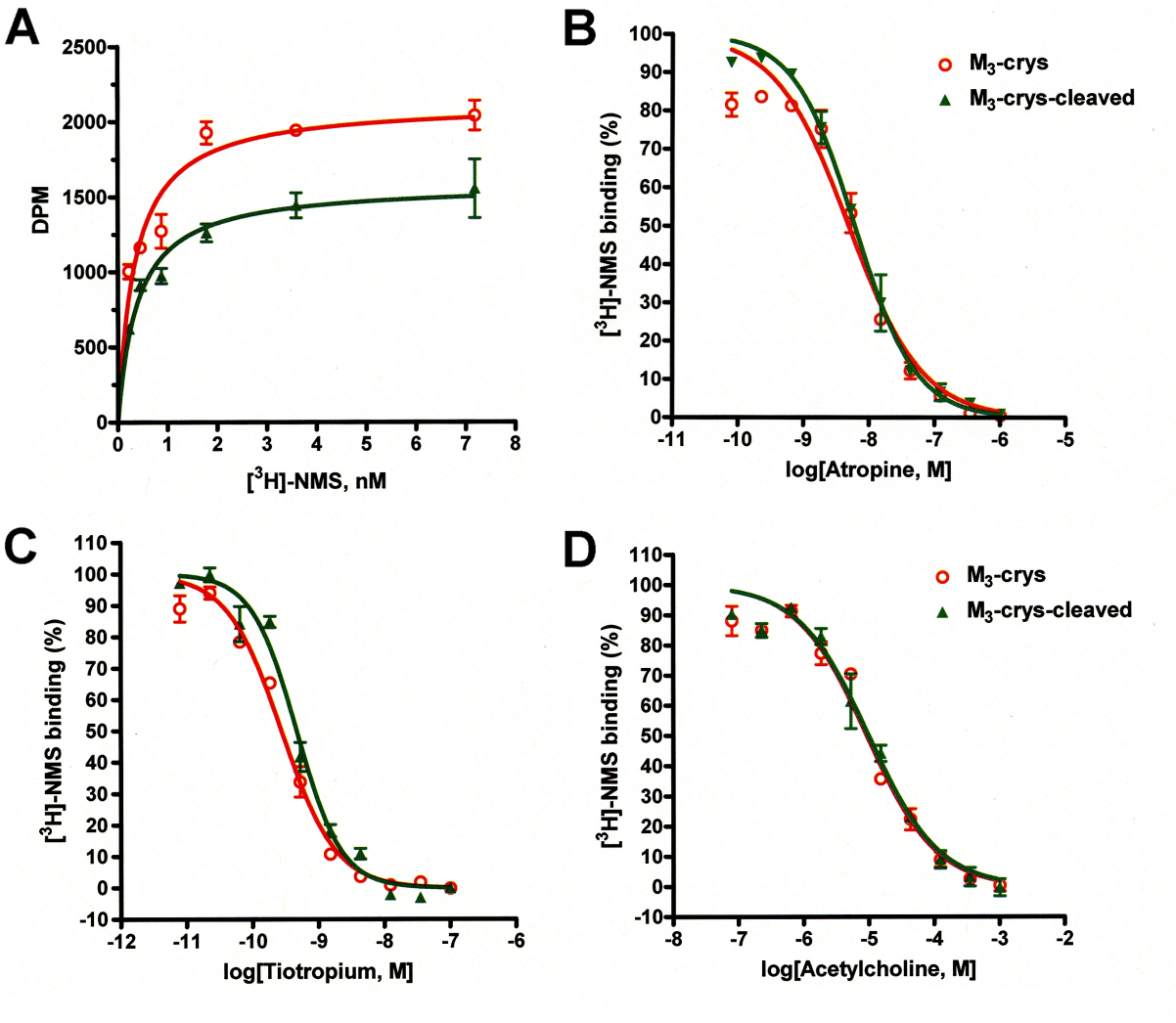

Figure S9. Cleavage of M_3-crys by TEV has no significant effect on ligand binding affinities. (**a**) Saturation binding curves of specific [^{3}H]NMS binding to the modified M_3 receptor construct used for crystallization studies (M_3-crys). In M_3-crys-cleaved, most of the extracellular N-terminal tail of M_3-crys was removed by cleavage with TEV (see Fig. S1). (**b**-**d**) Displacement of [^{3}H]NMS binding by atropine (**b**), tiotropium (**c**), and acetylcholine (**d**). Binding assays were carried out using membranes prepared from transfected COS-7 cells. The [^{3}H]NMS concentration used in the competition binding assays was 0.5 nM. Curves are representative of two or three independent experiments carried out in duplicate (for experimental details, see Online Methods). The two constructs yielded [^{3}H]NMS K_D values that were not significantly different from each other (M_3-crys, 337 ± 9 pM; M_3-crys-cleaved, 469 ± 110 pM).

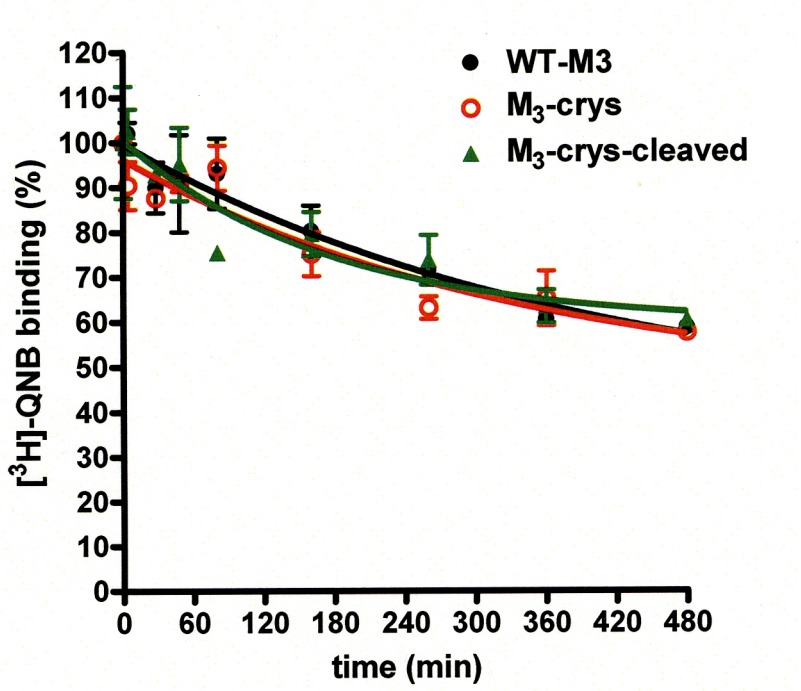

Figure S10. [^{3}H]-QNB dissociation rate assays. Experiments were carried out at 37 ^{o}C using membranes prepared from COS-7 cells transiently expressing the indicated M_3 receptor constructs. In M_3-crys-cleaved, most of the extracellular N-terminal tail of M_3-crys was removed by cleavage with TEV (see Fig. S1). At time t = 0, atropine (final concentration: 3 μM) was added and remaining [^{3}H]-QNB binding was determined at the indicated time points. Curves are representative of two independent experiments carried out in duplicate (for experimental details, see Online Methods).

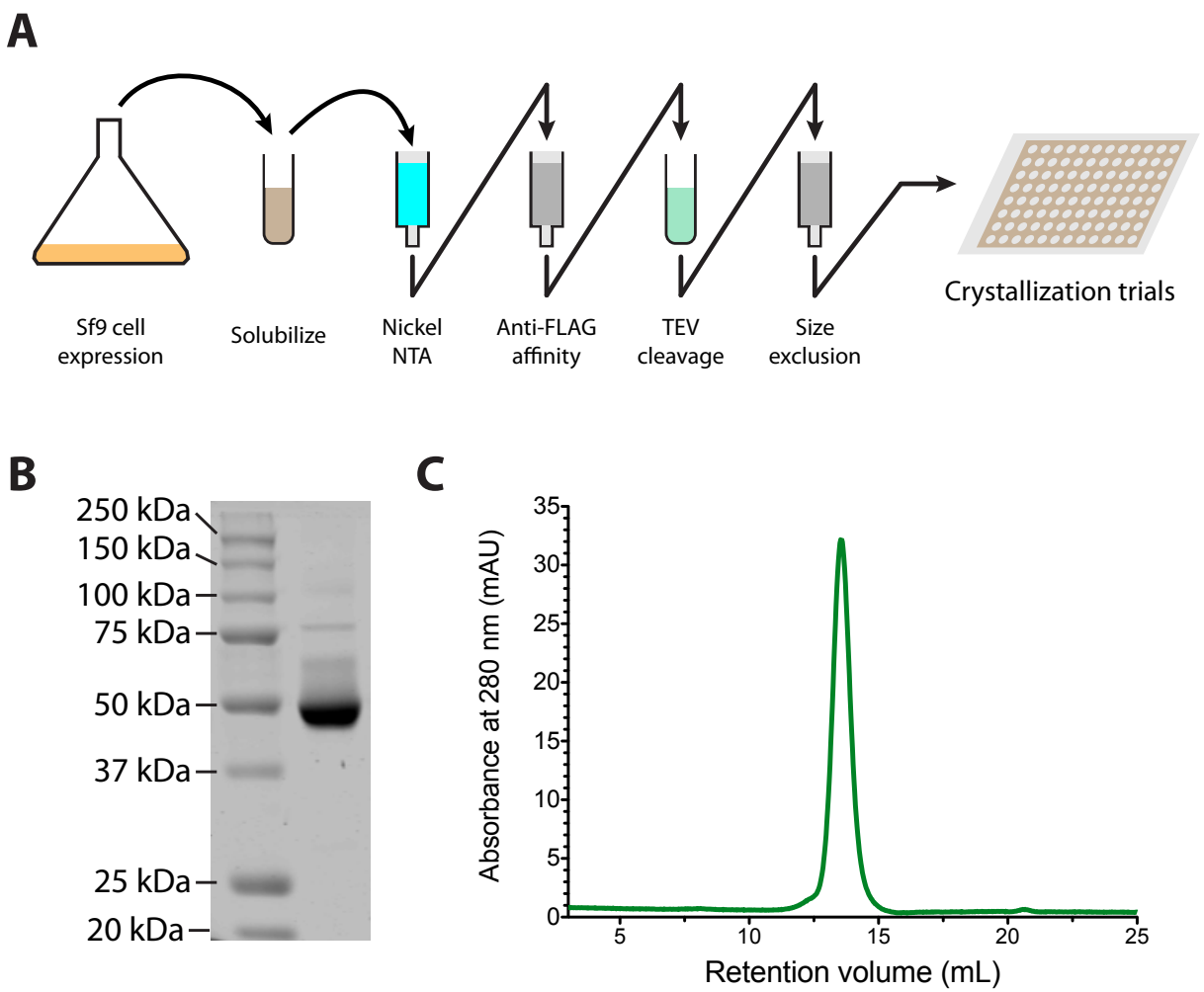

Figure S11. Purification of M_3 receptor. Receptor was purified by two affinity chromatography steps followed by size exclusion (**a**). SDS-PAGE analysis and analytical size exclusion show purity (**b**) and monodispersity (**c**) of a typical M_3 crystallization sample prepared in this way.

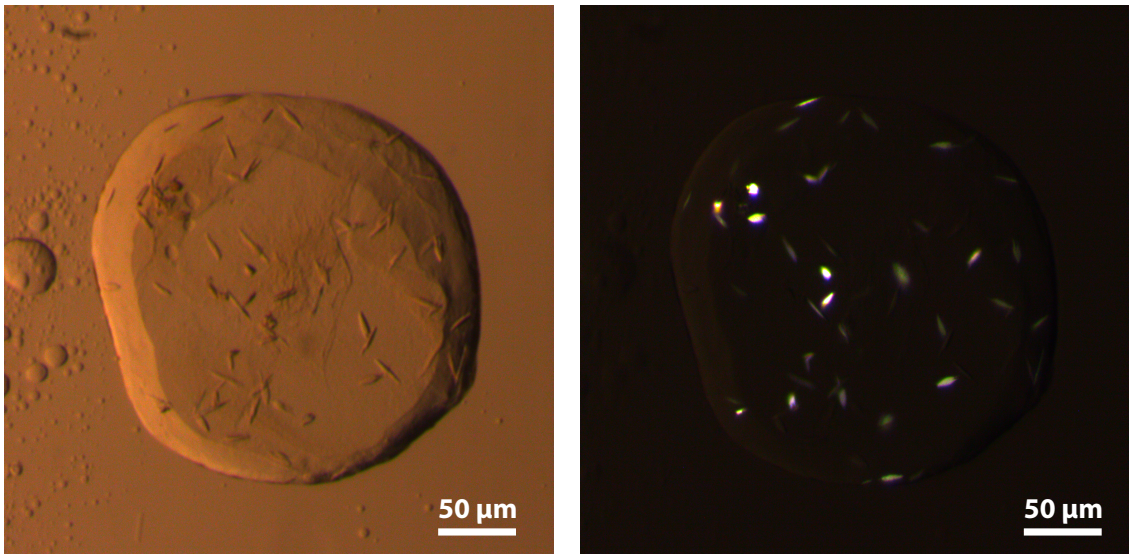

Figure S12. M_3 receptor crystals. Crystals are shown in bright field at left, and under crossed polarizers at right.

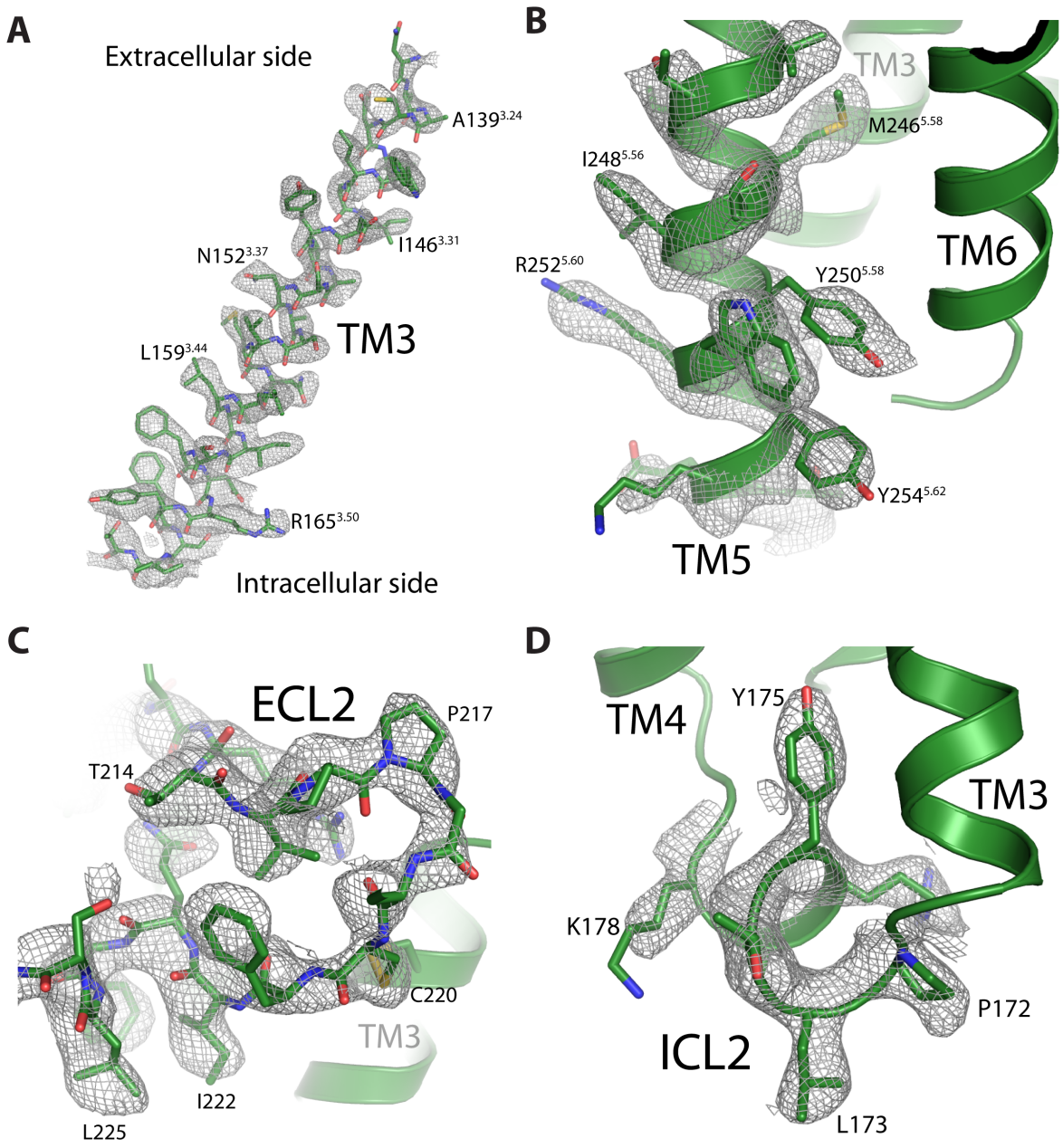

Figure S13. Representative electron density maps. A collection of representative NCS averaged electron density maps for different regions of the M_3 receptor. In each case, the map shown is a $2F_o$-F_c map contoured at 2 σ within 2.0 Å of the residues depicted in sticks. Regions shown are (**a**), the entirety of transmembrane helix 3 as oriented in the receptor when viewed parallel to the membrane, with several residues labeled for orientation, (**b**), the cytoplasmic end of transmembrane helix 5, (**c**), extracellular loop 2, and (**d**), intracellular loop 2.

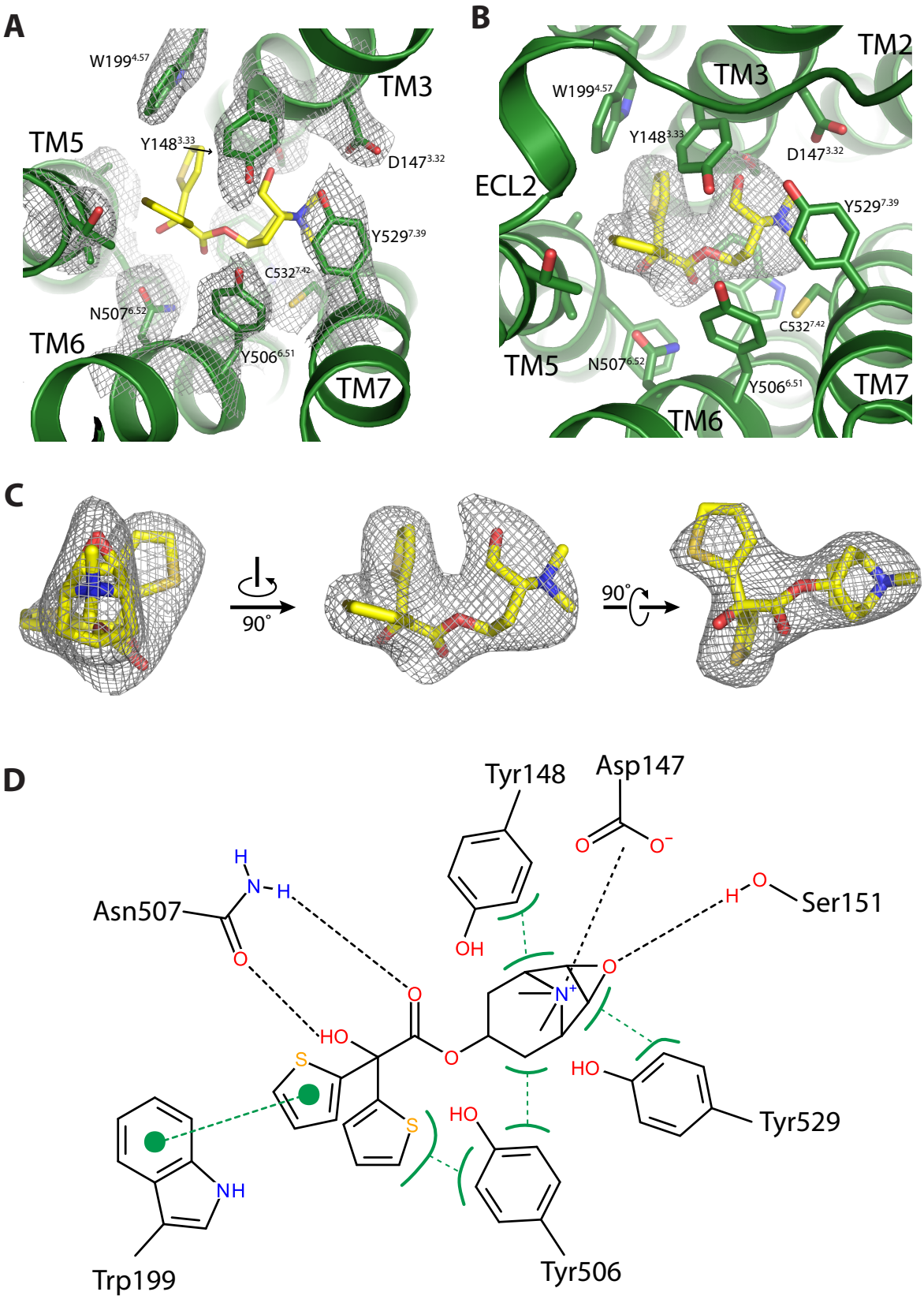
A
W199^4.57
TM3
TM5
Y148^3.33
D147^3.32
Y529^7.39
C532^7.42
N507^6.52
TM6
Y506^6.51
TM7
B
TM2
TM3
W199^4.57
Y148^3.33
D147^3.32
ECL2
Y529^7.39
C532^7.42
TM5
N507^6.52
Y506^6.51
TM7
TM6
C
90°
90°
D
Tyr148
Asp147
Asn507
Ser151
OH
HO
HO
HO
Tyr529
Trp199
Tyr506

Figure S14. Binding site electron density. The ligand tiotropium is bound in the orthosteric site of the M_3 receptor. Maps were calculated without non-crystallographic symmetry averaging. Interacting residues are shown in (**a**) as sticks with $2F_o$-F_c electron density maps contoured at 1.5 σ within 2 Å of each side chain. The binding site is shown again in (**b**) with an F_o-F_c tiotropium omit map contoured at 3 σ. For clarity, three views of the same map are shown for tiotropium in isolation in (**c**). In (**d**), the binding site is diagrammed with non-polar contacts shown in green, aromatic stacking with green circles, and polar contacts in black dotted lines. Any such two-dimensional diagram is necessarily a simplification of the three-dimensional binding site. Complete details of interactions are provided in supplementary table 3.

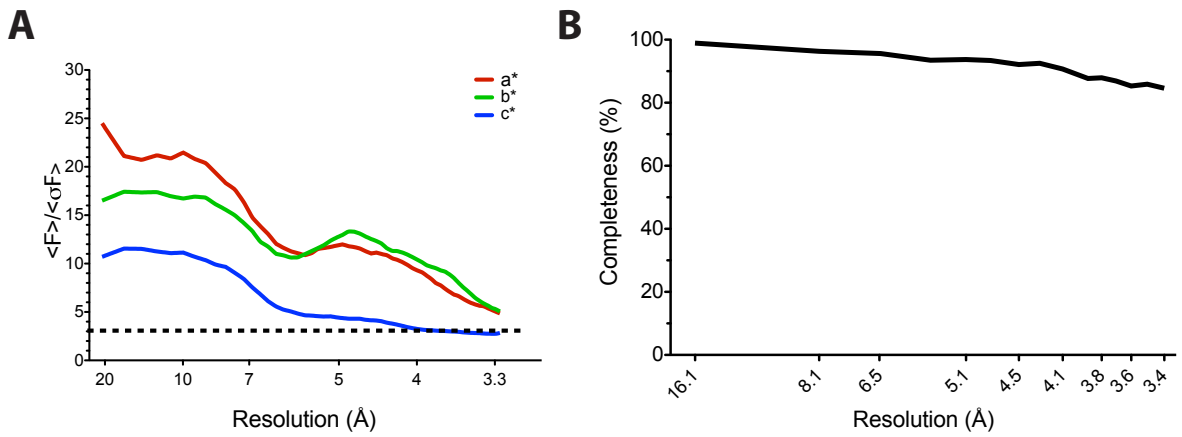

Figure S15. Analysis of diffraction data. A plot of <F>/<σF> against resolution of collected data in (**a**) shows that data quality along reciprocal space axes a* and b* is superior to that along c*. Due to this anisotropic diffraction and merging from multiple crystals, completeness decreases somewhat with resolution (**b**), but is similar to that of other GPCR structures. Data were subjected to anisotropic truncation to remove poorly measured reflections along c*, but NCS averaging largely compensates for this, giving highly interpretable electron density maps, as seen in figure S11. Complete data collection statistics are provided in supplementary table 1.

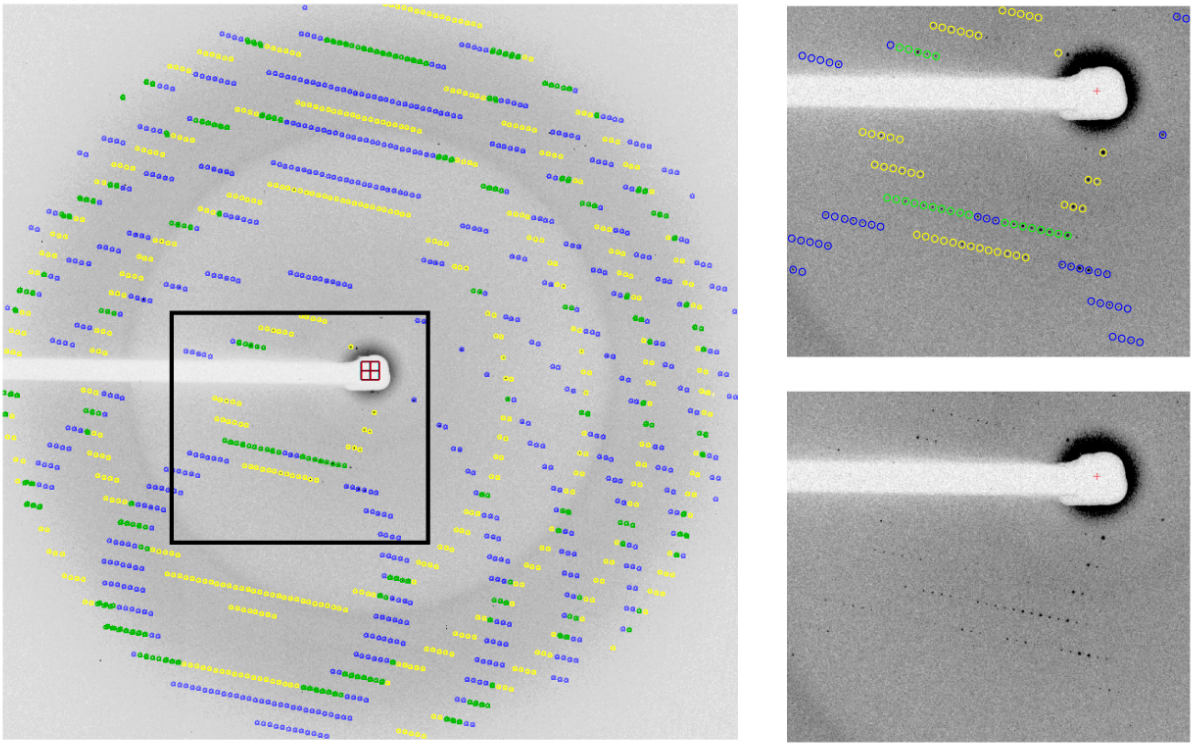

Figure S16. Evidence of epitaxial twinning. Diffraction of M_3 receptor crystals showed evidence of epitaxial twinning. Although many frames were dominated by a single lattice, in some cases two distinct lattices (see footnote to supplementary table 1) could be seen and indexed. Multiple lattices are commonly seen when many small crystals are included within a single loop. However, in this case spot predictions for the two lattices (blue and yellow) were not independent, but instead showed a clear geometric relationship, giving a combination of well-separated and overlapping spots (green). Such a mix of independent spots and precise superimposition is one hallmark of epitaxial twinning. The boxed region is shown in closeup view on the right, both with and without spot predictions.

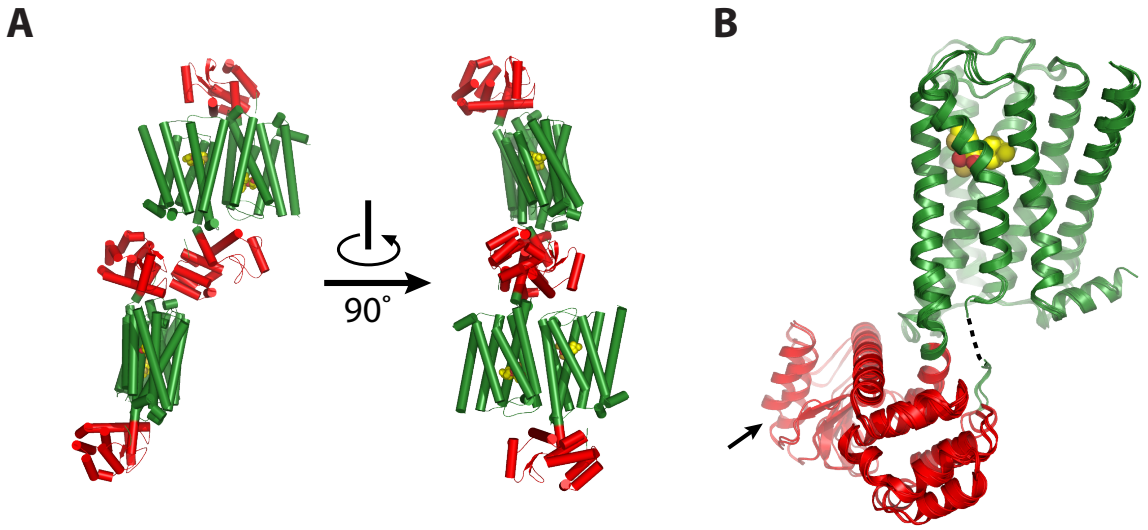

Figure S17. Non-crystallographic symmetry. The contents of the asymmetric unit (**a**) consist of four M_3 receptor molecules (green) each fused to a single T4 lysozyme molecule (red). (**b**) Superimposition of the four molecules shows relatively minor non-crystallographic deviations, with the exception of a pronounced shift in a lysozyme helix in two of the four molecules, indicated by an arrow.

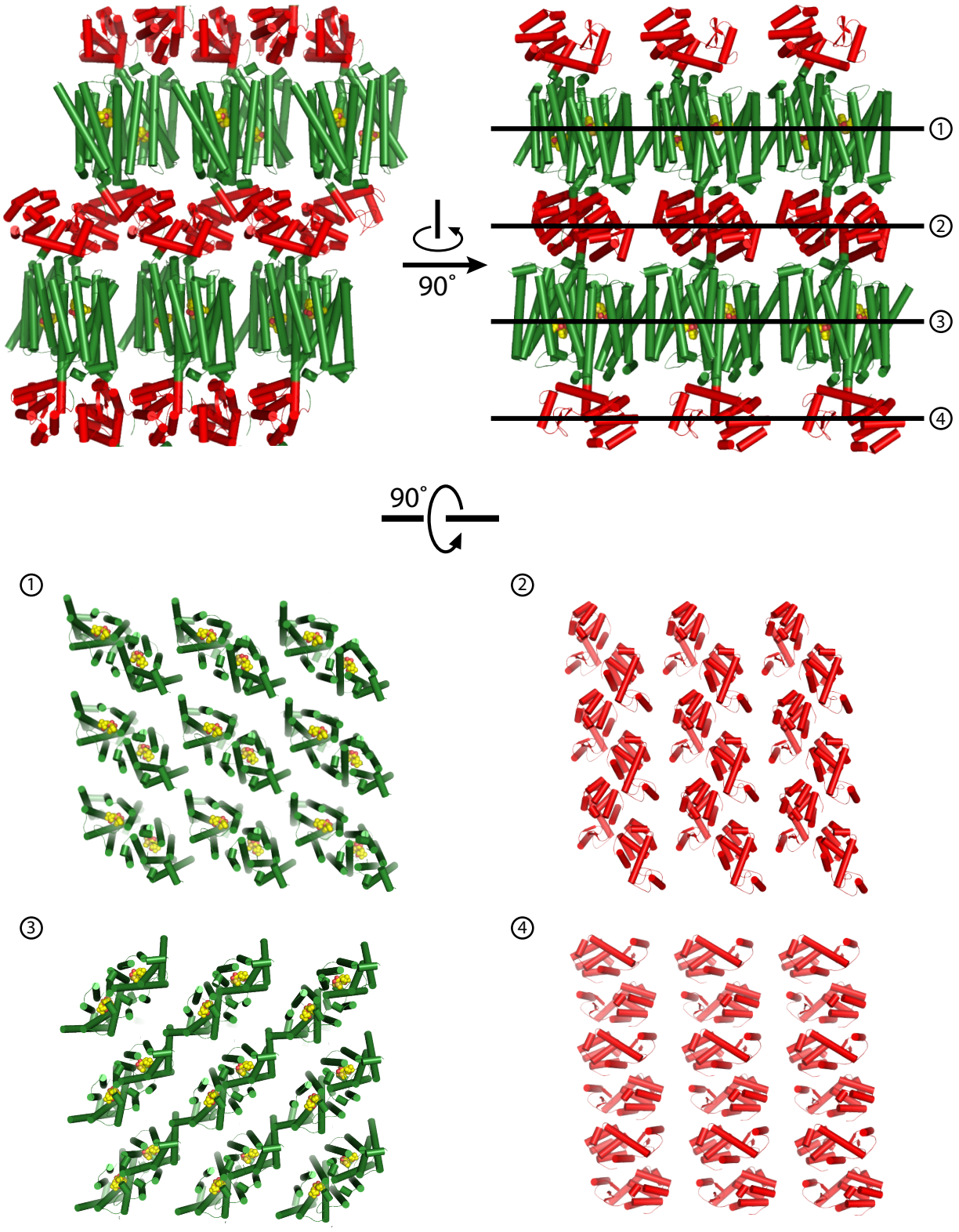

Figure S18. Lattice packing. M_3 receptor packs as antiparallel dimers, with two crystallographically unique aqueous and lipidic layers in each asymmetric unit. These four layers exhibit distinct lattice packings shown in the bottom of the figure.

Dimerization and oligomerization of M_3 receptors in cells has been reported previously[10-12], and the arrangement of the receptor molecules as pairs may be a reflection of an intrinsic propensity for association among mAChR monomers. However, the packing in the crystal is antiparallel and therefore cannot represent a physiological interface.

Using a combined BRET/mutagenesis approach, McMillin *et al.*[12] recently identified a series of M_3 receptor residues located on the outer surfaces of different TM helices that are predicted to play a role in M_3 receptor dimerization (oligomerization). In the X-ray structure of the M_3 receptor, these amino acids have very similar orientations as in the M_3 receptor model generated by McMillin *et al*. This observation is perhaps not very surprising since the M_3 receptor model was obtained by using the β_1 adrenergic receptor structure as a template (the two structures show a high degree of structural similarity within the TM helical bundle).

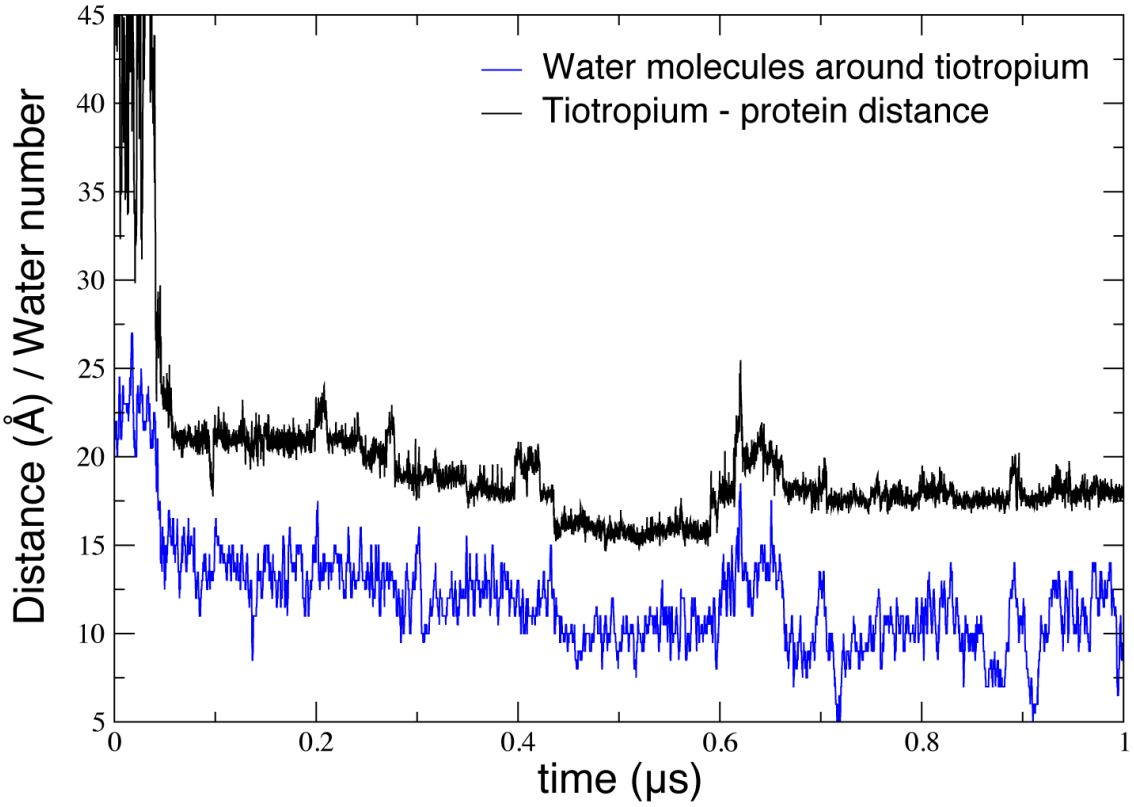

Figure S19. Tiotropium loses almost half of its hydration shell as it enters the extracellular vestibule. The black line is the distance between the centers-of-mass of tiotropium and the protein in a simulation of the M_3 receptor (Supplementary table 4, condition E), and the blue line is the number of water molecules within 3.6 Å of tiotropium's non-hydrogen atoms. The blue line has been smoothed with a 1.8 ns median filter. Similar behavior was observed in simulations of tiotropium entering the extracellular vestibule of the M_2 receptor (Supplementary table 4, condition D).

Supplementary table 1. Ligand binding properties of wild-type and modified M_3 receptor.

Receptor	[^{3}H] NMS		Atropine	Tiotropium	Acetylcholine	
	K_D	B_{max}	K_i	K_i	*Hill coefficient*	IC_{50}
	nM	*pmol/mg protein*	*nM*	*nM*		μM
WT M_3	0.75 ± 0.22	7.4 ± 1.3	5.9 ± 1.2	0.37 ± 0.02	0.75 ± 0.03	45.2 ± 14.4
M_3-crys	0.50 ± 0.27	16.6 ± 7.1	3.6 ± 0.5	0.27 ± 0.11	0.88 ± 0.19	7.7 ± 5.3

Radioligand binding studies were carried out using membranes prepared from COS-7 cells transiently expressing the wild-type M_3 receptor (WT M_3; rat) or the modified M_3 receptor construct used for crystallization studies (M_3-crys; see Fig. S1, S8). K_D and B_{max} values for [^{3}H]NMS were obtained in [^{3}H]NMS saturation binding assays. Affinity estimates (K_i values) for atropine and tiotropium, and IC_{50} values for acetylcholine were derived from [^{3}H]NMS competition binding assays (for experimental details, see Supplementary Methods). Antagonist binding curves showed Hill coefficients close to unity. Data are means ± SEM of 2-4 independent experiments carried out in duplicate.

The two receptors bound all antagonists with similar affinity. Interestingly, the M_3-crys construct bound the agonist acetylcholine with ~6-fold higher affinity compared to the WT M_3 receptor. This difference was not caused by receptor association with heterotrimeric G proteins, since inclusion of GTPγS (100 μM) in the incubation buffer had no significant effect on the position of the acetylcholine competition binding curves for either receptor (data not shown). Increased agonist affinity has also been reported previously for a β_2-adrenergic receptor-T4L fusion construct[13]. It is therefore likely that replacement of the third intracellular loop with T4 sequence (in M_3-crys) causes an increase in acetylcholine binding affinity via an allosteric effect.

Supplementary table 2. Data collection and refinement statistics.

Data collection[a]	
Number of crystals	76
Space group	P 1
Cell dimensions[b]	
a, b, c (Å)	54.8, 61.3, 176.9
α, β, γ (°)	85.9, 89.9, 84.9
Resolution (Å)	39.9 – 3.4 (3.5 – 3.4)
R_{merge} (%)	22.6 (52.7)
$\langle I \rangle / \langle \sigma I \rangle$	4.5 (1.7)
Completeness (%)	90.6 (85.9)
Redundancy	3.7 (2.8)
Refinement	
Resolution (Å)	39.9 – 3.4
No. unique reflections	26013 (1276 in test set)
R_{work}/R_{free} (%)	25.1 / 30.3
Anisotropic *B* tensor	B_{11}= -2.2 / B_{22}= 6.6 / B_{33}= -4.4 / B_{12}= 2.0 / B_{13}= 0.1 / B_{23}= -1.3
Average *B*-factors (Å^2)	
M_3 muscarinic receptor	88.2
Tiotropium	69.9
T4 lysozyme	87.4
R.m.s. deviation from ideality	
Bond length (Å)	0.01
Bond angles (°)	0.86
Ramachandran statistics[c]	
Favored regions (%)	94.4
Allowed regions (%)	6.6
Outliers (%)	0

[a]Highest shell statistics are in parentheses. [b]Dimensions of the second (poorly diffracting) twin were identical, but with axes *a* and *c* switched. [c]As defined by MolProbity[14].

Supplementary Table 3. List of receptor ligand contacts

M_3 receptor	**Tiotropium**	**Closest contact (Å)**[a]
Ser151 hydroxyl	Epoxide ether oxygen	2.9
Asp147 carboxylate	Amine	4.3
Asn507 NH_2	Carbonyl	3.5
Asn507 carbonyl	Hydroxyl	3.3
Cys532 Cβ	Tropane	2.9
Tyr529 aromatic ring	Tropane	3.6
Tyr506 aromatic ring	Tropane	3.9
Tyr148 aromatic ring	Tropane	3.3
Trp503	Tropane	3.8
Asn152 Cα, Cβ	Thiophene 1	3.6
Trp199 indole	Thiophene 1	3.6
Ala235 Cα	Thiophene 2	3.7
Thr231 Cγ	Thiophene 2	3.9

[a]The closest contacts for residues potentially interacting with tiotropium in the refined crystal structure of the M_3 receptor are listed. [b]Thiophene 1 denotes the deeply buried thiophene ring closer to the cytoplasmic side of the receptor, while thiophene 2 denotes the thiophene nearer to the extracellular surface.

Simulations with bound ligands

Condition	Receptor	Ligand	Number	Durations (μs)
A	M_2	QNB	1	16.4
B	M_2	Tiotropium	1	13.9
C	M_3	Tiotropium	1	10.2

Spontaneous binding simulations

Condition	Receptor	Ligand	Number	Durations (μs)	Total binding events
D	M_2	4 tiotropium molecules	3	14.2, 1.0, 1.0	10 (extracellular vestibule)
E	M_3	4 tiotropium molecules	3	16.0, 1.0, 1.0	7 (extracellular vestibule)
F	M_3	4 acetylcholine molecules	1	25.0	1 (orthosteric binding pocket)

Forced dissociation simulations

Condition	Receptor	Ligand	Number	Durations (μs)
G	M_2	Tiotropium	7	1.0, 1.0, 1.0, 1.0, 1.0, 1.0, 1.0
H	M_3	Tiotropium	7	1.0, 1.0, 1.0, 1.0, 1.0, 1.0, 1.0

Supplementary table 4. Molecular dynamics simulations "Number" indicates number of independent simulations under each condition. In the spontaneous binding simulations with tiotropium, ligands bound to and dissociated from the extracellular vestibule multiple times, but never entered the orthosteric binding pocket (presumably because the simulations were not sufficiently long). An acetylcholine molecule did bind in the orthosteric binding pocket. See Online Methods for details.

Literature cited

1. Scarselli, M., Li, B., Kim, S.-K. & Wess, J. Multiple residues in the second extracellular loop are critical for M_3 muscarinic acetylcholine receptor activation. *J. Biol. Chem.* **282**, 7385-7396 (2007).
2. Goodwin, J.A., Hulme, E.C., Langmead, C.J., & Tehan B.G. Roof and floor of the muscarinic binding pocket: variations in the binding modes of orthosteric ligands. *Mol Pharmacol.* **72,** 1484-1496 (2007).
3. Matsui, H., Lazareno, S. & Birdsall. N.J.M. (1995) Probing of the location of the allosteric site on M_1 muscarinic receptors by site-directed mutagenesis. *Mol. Pharmacol.* **47**, 88-98.
4. Li, B. *et al.* Rapid identification of functionally critical amino acids in a G protein-coupled receptor. *Nat. Methods* **4**, 169-174 (2007).
5. Schmidt, C. *et al.* Random mutagenesis of the M_3 muscarinic acetylcholine receptor expressed in yeast. *J. Biol. Chem.* **278**, 30248-30260 (2003).
6. Rasmussen, S. G. F. *et al.* Crystal structure of the β_2 adrenergic receptor-Gs protein complex. *Nature* **477**, 549-555 (2011).
7. Hu, J. *et al.* Structural basis of G protein-coupled receptor-G protein interactions. *Nat. Chem. Biol.* **6**, 541-548 (2010).
8. Moro, O., Lameh, J., Högger, P. & Sadée, W. Hydrophobic amino acid in the i2 loop plays a key role in receptor-G protein coupling. *J. Biol. Chem.* **268**, 22273-22276 (1993).
9. Eswar, N. *et al.* in *Current Protocols in Bioinformatics. 15:5.6.1–5.6.30* (John Wiley & Sons, Inc., 2006).
10. Zeng, F.-Y. & Wess, J. Molecular aspects of muscarinic receptor dimerization. *Neuropsychopharmacology* **23**, S19-S31 (2000).
11. Hern *et al.* Formation and dissociation of M_1 muscarinic receptor dimers seen by total internal reflection fluorescence imaging of single molecules. *Proc. Natl. Acad. Sci.* **107**, 2693-2698 (2010).
12. McMillin *et al.* Structural basis of M_3 muscarinic receptor dimer/oligomer formation. *J. Biol. Chem.* **286**, 28584-28598 (2011)
13. Rosenbaum, D.M. *et al.* GPCR engineering yields high-resolution structural insights into β_2-adrenergic receptor function. *Science* **318**, 1266–1273 (2007).
14. Davis, I. W., Murray, L. W., Richardson, J. S. & Richardson, D. C. MolProbity: structure validation and all-atom contact analysis for nucleic acids and their complexes. *Nucleic Acids Res.* **32**, W615-W619 (2004).